JOURNAL OF SPACECRAFT AND ROCKETS
Vol. 42, No. 3, May–June 2005

Rapid Engineering Approach to Modeling Hypersonic Laminar-to-Turbulent Transitional Flows

J. L. Papp* and S. M. Dash†
Combustion Research and Flow Technology, Inc., Pipersville, Pennsylvania 18947

Modeling the transitional behavior of hypersonic flows from an engineering point of view is addressed. More specifically, the accuracy of transition onset predictions by using a modified transition onset transport model is examined. Transitional blending is predicted by using the well-established Dhawan and Narasimha algebraic model. To employ the rapid engineering approach, the methodology is encompassed within the So, Sarkar, Gerodimos, and Zhang low-Reynolds-number k–ε turbulence model framework that has been extended to include compressibility effects. Model calibration and validation is achieved by using fundamental flat-plate data sets of Mee as well as recent data sets obtained by Holden for scramjet forebody geometries. It is shown that the transition onset transport equation predicts onset in accord with experimental values by using freestream velocity fluctuation levels consistent with those of the shock tunnel facilities. An additional simulation of the reentry F vehicle under low noise flight conditions was also performed. Under these conditions, the onset model predicts the location of transition very close to that measured. Overall, the framework developed can be used for very rapid turnaround engineering applications. The model can account for both freestream noise as well as amplification effects caused by shock/boundary interactions, specifically those dealing with compression corners.

Nomenclature

c_H	=	heat-transfer coefficient, $=q_w/\rho_e U_e c_{p_e}(T_{\text{aw}} - T_w)$
c_p	=	specific heat at constant pressure, J/kg-K
k	=	turbulent kinetic energy, m^2/s^2
k_L	=	laminar fluctuation component of turbulent kinetic energy, m^2/s^2
M	=	boundary-layer edge Mach number
M_T	=	turbulent Mach number
$\tilde{M}_T$	=	effective turbulent Mach number
$\hat{n}\sigma\|_{\text{ZPG}}$	=	zero-pressure-gradient turbulent spot formation parameter
P	=	gas pressure, Pa
q	=	heat transfer, W/m^2
Re	=	Reynolds number
Re_{θ_t}	=	momentum thickness Reynolds number, $=\rho_\infty U_\infty \theta_t/\mu_\infty$
R_T	=	transition onset parameter, $=1/C_\mu(\mu_{T_\ell}/\mu)$
r	=	adiabatic wall-temperature recovery factor
T	=	temperature, K
T_{aw}	=	adiabatic wall temperature, K, $=T_e\{1 + r[(\gamma-1)/2]M_e^2\}$
Tu	=	freestream velocity fluctuation level, $=\sqrt{(\frac{2}{3}k_\ell)}/U_\infty \cdot 100$
U	=	gas velocity, m/s
u	=	gas velocity, m/s
x_f	=	fully turbulent streamwise location, m
x_t	=	transition onset streamwise location, m
Γ	=	turbulent intermittency
γ	=	specific heat ratio
ε	=	turbulent dissipation rate, m^2/s^3
μ	=	laminar eddy viscosity, N-s/m^2
μ_T	=	turbulent eddy viscosity, N-s/m^2
$\tilde{\mu}_T$	=	effective turbulent eddy viscosity, N-s/m^2
$\tilde{\mu}_T\omega$	=	instability mode timescale, 1/s
μ_{T_ℓ}	=	laminar fluctuation component of turbulent eddy viscosity, N-s/m^2
ρ	=	gas density, kg/m^3
θ	=	momentum thickness, m
$\bar{\bar{\tau}}$	=	turbulent Reynolds-stress tensor, N/m^2

Subscripts

e	=	boundary-layer edge conditions
i, j, k	=	tensor indices
T	=	turbulent condition
t	=	transition onset location
w	=	wall conditions
∞	=	freestream conditions

Superscripts

‘	=	fluctuating value
$*$	=	reference temperature correlation values

Introduction

TRANSITIONAL phenomena play an important role in hypersonic flows for applications encompassing reentry vehicles, scramjets, tactical and ballistic missiles, and interceptor missiles with divert jets. The marked differences in skin friction and heat transfer for flows that are fully laminar, fully turbulent, or transitional can have a profound impact on design characteristics and vehicle performance. Many experiments have been performed to gain an understanding of the physical mechanisms controlling transition and to support modeling methodologies to predict transitional behavior.

As our knowledge of the transition mechanisms has grown, so to have the numerical models used to predict transition. Early empirical models that used experimental correlations have been succeeded by more complex methods based on the growth of instability modes. Initially, only linear modes were simulated, but increased computer power has allowed for the simulation of more complex nonlinear modes, to obtain yet more accurate transition onset predictions. These e^N methods represent the cutting edge in transition prediction

Presented as Paper 2002-0155 at the AIAA 40th Aerospace Sciences Meeting, Reno, NV, 14–17 January 2002; received 10 April 2003; revision received 29 January 2004; accepted for publication 2 February 2004.

*Research Scientist, 6210 Keller's Church Road; jpapp@craft-tech.com. Member AIAA.

†President and Chief Scientist, 6210 Keller's Church Road. Associate Fellow AIAA.

and are approaching a level at which engineering applications are feasible, especially with the recent development of LASTRAC.[1] However, this first-principals oriented fidelity comes at the price of complexity and large CPU requirements and is not yet proven for complex three-dimensional flowfields.

To prevent spurious mode growth as a consequence of numerical inaccuracy with stability based methods, a high-fidelity and often time-consuming flowfield simulation is required to permit extracting the correct instability growth rate trends. For most applications of engineering interest at the systems level, rapid turnaround time and much less stringent requirements on solution accuracy are required. Thus, one- and two-equation turbulence models are used in engineering applications as opposed to more complex, full Reynolds-stress models. Improved physics is sacrificed for simplicity and robustness as long as solutions are adequate for the application at hand. Similarly, when it comes to modeling transition onset and transition to turbulence engineering methodologies have maintained links to simplicity and robustness through use of experimental correlations or through a turbulence modeling framework that incorporates limited transitional physics.

In this paper, a practical engineering methodology for the prediction of hypersonic transitional flows is examined by using conventional Reynolds-averaged Navier–Stokes (RANS) numerics. There are several aspects to the overall hypersonic transitional modeling process that include 1) onset prediction, 2) laminar-to-turbulent transitional blending, and, 3) inclusion of high-Mach-number compressibility effects. Ultimately, these require unification within a RANS turbulence modeling framework that minimizes often complex user intervention, with emphasis on the use of parabolized Navier–Stokes (PNS) solution methodology that can provide complete problem turnaround in minutes.

Turbulence Modeling and Transitional Considerations

Numerical procedures for transition blending from laminar to fully turbulent flow are based on intermittency concepts. Some basis in the physics of transition is afforded by modeling turbulent spot production in some manner, resulting in the eventual transition to full turbulence. In general, intermittency is a three-dimensional, time-varying phenomenon. However, most simplified models assume a steady-state variation in only a single dimension, typically the streamwise or flow direction.

The well-established method for simulating transitional behavior within a RANS approach is to suppress turbulence in regions that are fully laminar and gradually blend turbulence into regions that are transitional. Because the direct effect of turbulence for a RANS approach is incorporated through the turbulent eddy viscosity (TEV), an effective turbulent eddy viscosity is defined as

$$\tilde{\mu}_T = \Gamma \mu_T \tag{1}$$

and is used in lieu of the actual TEV in the RANS equation set. The transition intermittency function Γ is zero in regions of fully laminar flow and varies between zero at onset and unity in the turbulent region. Because the current interest is in modeling the transition from laminar-to-turbulent flow and not in other complexities associated with relaminarization, Γ is assumed to remain unity downstream of regions that have evolved into fully developed turbulent flow.

Because the entire transitional process is represented through the Γ function, the turbulence model itself must exhibit no pseudotransitional behavior. Some low-Reynolds-number near-wall models contain near-wall damping terms that can behave in an unpredictable manner and can be highly dependent on near-wall grid resolution and flow conditions. Slight changes can suddenly turn a nominally well-behaved turbulence model into one that exhibits transitional-like behavior. As an example, shown in Fig. 1 are comparisons between two turbulence models for flow over an adiabatic flat plate at Mach 6.2. Grid 1 has a near-wall spacing of 1.0×10^{-8}, whereas grid 2 has a near-wall spacing of 1.0×10^{-6}. The SSGZ-J model of So et al.[2] predicts fully turbulent flow for both cases, whereas the Chien model[3] exhibits pseudotransitional features that are highly grid dependent.

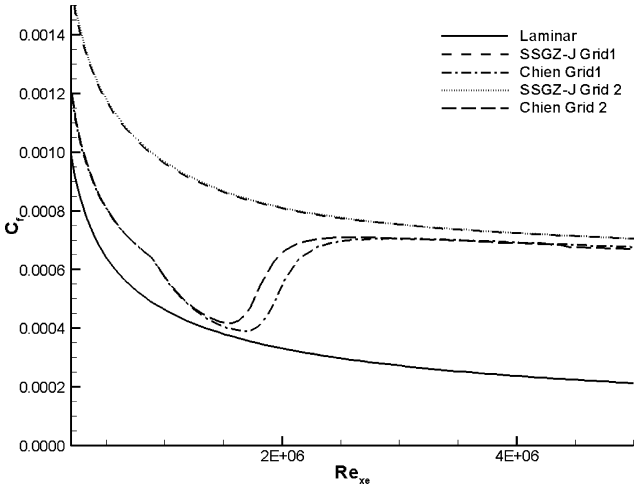

Fig. 1 Example of pseudotransitional behavior of near-wall model.

Based on several exploratory studies, Fig. 1 being but one example, the So et al.[2] (SSGZ) k–ε model has been found to behave predictably within the near-wall region for transitional flows. Incorporating knowledge gained from DNS studies, the model also reproduces correct near-wall turbulence trends for various wall-dominated flows.[2,4] The model does not introduce any wall specific dependencies, such as y^+, making it readily applicable to complex geometries and unstructured grid methodologies. A modified variant of the SSGZ model, SSGZ-J, has been used extensively by the present authors and has been calibrated for hypersonic flows by using improved compressibility correction techniques.[5] Considering these issues, the SSGZ-J model is chosen to perform all simulations in the present paper.

Compressibility-Corrected SSGZ-J k–ε Model

The modified SSGZ-J governing equations are

$$\frac{\partial \rho k}{\partial t} + \rho u_j \frac{\partial k}{\partial x_j} - \frac{\partial}{\partial x_j}\left[\left(\mu + \frac{\mu_T}{\sigma_k}\right)\frac{\partial \rho k}{\partial x_j}\right] = P_k - D_k + SS_k \tag{2}$$

$$\frac{\partial \rho \varepsilon}{\partial t} + \rho u_j \frac{\partial \varepsilon}{\partial x_j} - \frac{\partial}{\partial x_j}\left[\left(\mu + \frac{\mu_T}{\sigma_\varepsilon}\right)\frac{\partial \rho \varepsilon}{\partial x_j}\right] = P_\varepsilon - D_\varepsilon \tag{3}$$

where

$$P_k = \tau_{ij}\frac{\partial u_i}{\partial x_j} \tag{4}$$

$$D_k = \rho \varepsilon \tag{5}$$

$$P_\varepsilon = C_{\varepsilon_1} P_k \frac{\varepsilon}{k} \tag{6}$$

$$D_\varepsilon = C_{\varepsilon_2} \varepsilon \frac{\varepsilon}{k} \tag{7}$$

$$\tau_{ij} = -\bar{\rho}\overline{u_i' u_j'} \tag{8}$$

$$S_{ij} = \frac{1}{2}\left(\frac{\partial u_i}{\partial x_j} + \frac{\partial u_j}{\partial x_i}\right) \tag{9}$$

$$\mu_T = C_\mu \rho \frac{k^2}{\varepsilon} \tag{10}$$

with closure coefficients given by $C_{\varepsilon_1} = 1.50$, $C_{\varepsilon_2} = 1.83$, $C_\mu = 0.09$, $\sigma_k = 1.0$, and $\sigma_\varepsilon = 1.44$.

Compressibility effects are introduced through additional source terms, which have been calibrated for supersonic and hypersonic flows.[5] In particular, a variant of the Sarkar[6] and Zeman[7,8] compressible-dissipation/pressure-dilatation model is implemented

to account for compressibility effects, with the source term defined as

$$SS_k = -\alpha_1 \tilde{M}_T^2 P_k - \alpha_2 \tilde{M}_T^2 \rho\varepsilon \tag{11}$$

where

$$\tilde{M}_T = \max(M_T - \lambda, 0) \tag{12}$$

is an effective turbulent Mach number having a lag λ to suppress compressibility effects for values of $M_T < 0.2$. This same compressibility correction is used for ducted flows and free shear flows.[5] The closure coefficients used are

$$\alpha_1 = 2.5, \qquad \alpha_2 = 2.0, \qquad \lambda = 0.2 \tag{13}$$

The importance of compressibility corrections at hypersonic speeds is made evident by the comparisons of skin friction at various Mach numbers over an isothermal, cold ($T_w/T_e = 1.0$) flat plate, shown in Fig. 2.

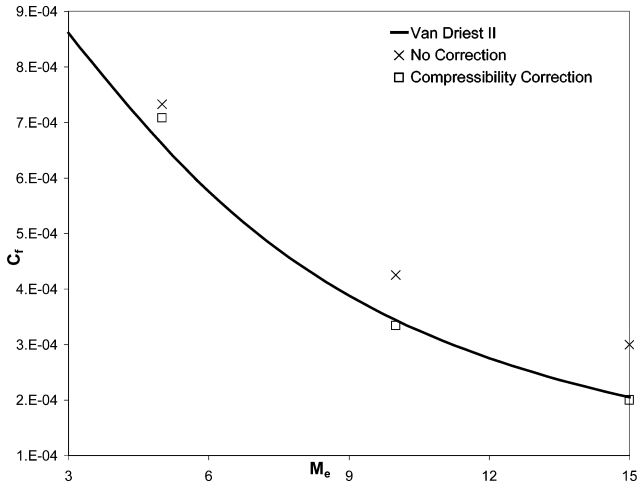

Fig. 2 Effect of compressibility on predicted skin-friction values for isothermal wall.

Overview of Experimental Wind-Tunnel Validation Cases

Transitional data for hypersonic flows over cones and reentry vehicle (RV)-like bodies are readily available and transition prediction, and model calibration for these cases has been reported with use of correlative models.[9] The focus here is on the application of the transition onset model of Warren et al.[10] unified with the SSGZ-J k–ε model with a compressibility correction for hypersonic scramjet and missile applications. Recent high-speed flat plate studies of Mee[11] and hypersonic scramjet forebody experiments of Holden and Rodriguez[12] and Holden[13] at the CUBRC LENS facility are chosen as the validation cases. Because all of the experiments were performed in shock tunnels with relative short test times, cold-wall conditions ($T_w = 300$ K) are assumed.

Flow conditions for cases analyzed are summarized in Table 1. In the flat-plate cases of Mee, the numerical simulations assume a sharp nose. Schematics of forebody geometries for the scramjet cases are shown in Figs. 3 and 4. Unfortunately, freestream noise levels are not measured for any of the experiments. Pressure fluctuation measurements reported for varied shock tunnels have typically ranged from 1 to 8% (Ref. 14), and these are used as guidelines to determine applicable turbulence intensity conditions.

Experimental error in heat-transfer coefficient for the Mee study is estimated to be ±18% (Ref. 15). Error estimates for the Holden

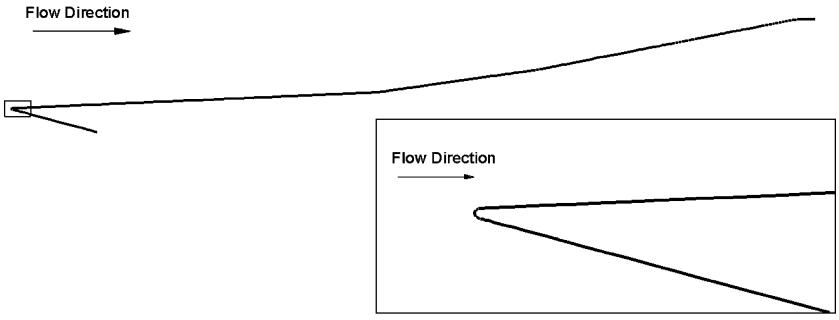

Fig. 3 Holden RUN 3/5 geometry with blowup of nose region.

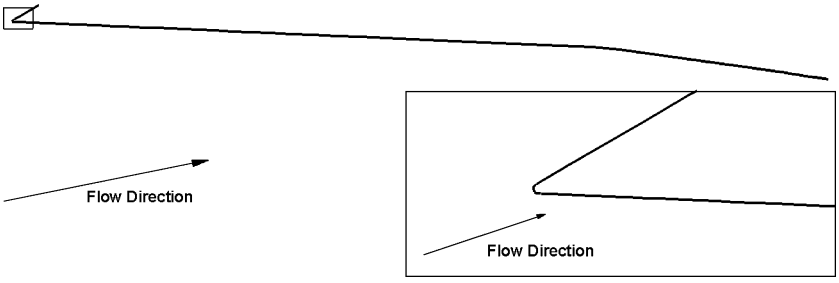

Fig. 4 Holden RUN 77/81 geometry with blowup of nose region.

Table 1 Experimental case conditions

Experiment	Designation	Conditions	Geometry
Mee[11]	Shot 6909/6910	$M_\infty = 6.2$, $p_\infty = 5.4 \times 10^3$ Pa, $T_\infty = 690$ K, $Re = 2.6 \times 10^6$ m^{-1}, 0-deg AOA[a]	Sharp nose flat plate
Mee[11]	Shot 6912/6913	$M_\infty = 6.1$, $p_\infty = 12.1 \times 10^3$ Pa, $T_\infty = 800$ K, $Re = 4.9 \times 10^6$ m^{-1}, 0-deg AOA	Sharp nose flat plate
Holden[13]	RUN 3	$M_\infty = 10.3$, $p_\infty = 814$ Pa, $T_\infty = 225$ K, $Re = 2.7 \times 10^6$ m^{-1}, 1 deg AOA	Fig. 3
Holden[13]	RUN 5	$M_\infty = 10.6$, $p_\infty = 832$ Pa, $T_\infty = 215$ K, $Re = 3.0 \times 10^6$ m^{-1}, 1-deg AOA	Fig. 3
Holden[13]	RUN 77	$M_\infty = 7.2$, $p_\infty = 1.70 \times 10^3$ Pa, $T_\infty = 207$ K, $Re = 4.3 \times 10^6$ m^{-1}, 6-deg AOA	Fig. 4
Holden[13]	RUN 81	$M_\infty = 7.2$, $p_\infty = 1.83 \times 10^3$ Pa, $T_\infty = 208$ K, $Re = 4.6 \times 10^6$ m^{-1}, 6-deg AOA	Fig. 4

[a]AOA = angle of attack.

experiments were not specifically reported, but similar experiments within the facility estimated errors of around ±15% (Ref. 12). As a further estimate of experimental error, multiple experimental measurements at nearly the same test conditions are given for each case.

The primary means of comparison between experiment and simulation is either through the direct heat-transfer rate or through the heat-transfer coefficient defined as

$$c_H = q_w \Big/ \rho_e U_e c_{p_e} (T_{\text{aw}} - T_w) \tag{14}$$

where

$$T_{\text{aw}} = T_e \left\{ 1 + r[(\gamma - 1)/2] M_e^2 \right\} \tag{15}$$

The recovery factor r is assumed to be unity in all cases.

Simulation Methodology

Simulations described in this paper are performed by using the CRAFT CFD® full RANS structured flow solver.[16] The CRAFT CFD code uses a finite volume second-order spatially accurate approach with a third-order spatially accurate upwind-biased total-variation-diminishing scheme for the numerical fluxes. All equations are solved fully coupled. Because the flow is largely supersonic, the parabolized form of the Navier–Stokes equation set is utilized to speed up turnaround times and minimize CPU requirements. Standard Vigneron sublayer methods are implemented to deal with the subsonic boundary layer. Air is the working medium for all simulations and disassociation, or thermal nonequilibrium is assumed to be negligible.

Each case is converged to machine accuracy and is performed on multiple grid levels to ensure grid independence. All cases, except for very small regions near any blunt leading edges, are performed using the PNS methodology. Consequently, the number of grid points in the streamwise direction is irrelevant as this is governed by the convergence criteria. Grid-convergence studies need only examine the effect of near-wall spacing and number of transverse points.

A total of three mesh sizes (257, 129, 65 transverse points) for two near-wall spacing configurations (1×10^{-6} and 1×10^{-8} m) are examined to analyze grid convergence. The finest mesh for each wall clustering configuration is generated using a hyperbolic tangent clustering approach.[17] A schematic of a typical grid is shown Fig. 5. Each coarser mesh is then generated by removing ever other point from the next finer mesh resulting in a refinement factor of 2. Although CRAFT CFD is a second-order accurate solver, the first-order boundary conditions lower the accuracy to near 1.5.

A Richardson extrapolation can now be used to estimate grid error. Two criteria are used to determine grid dependency, predicted transition onset location, and wall heat transfer. Although grid convergence is scrutinized for all cases presented, only Shot 6912/6913 of Mee is used here as an example. Table 2 summarizes the grid error for the transition location. Grid convergence is achieved by using the 129-point grid for both near-wall spacing values. Even the coarsest mesh is within 5% of the estimated result. Grid error for heat transfer is shown in Figs. 6 and 7. Estimated grid errors are well below 1% for 1×10^{-8} m near-wall spacing when using at least 129 transverse points. Because the bulk of the simulations performed use the efficient PNS space marching scheme, at least 257 points in the transverse direction and 1×10^{-8} m or less near-wall spacing are used for all simulation results presented.

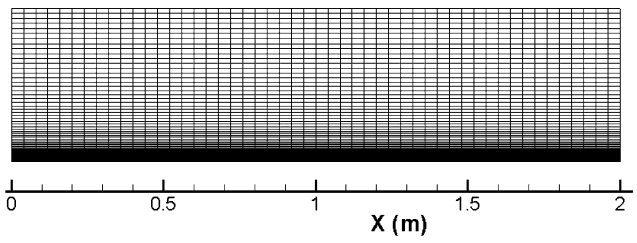

Fig. 5 Grid topology example for grid-dependency study.

Intermittency Modeling of Transition to Turbulence

Although several methods for modeling intermittency exist based on experimental correlations, perhaps the most widely used is that developed by Dhawan and Narasimha.[18] The basic model has been applied primarily to low-speed zero-pressure-gradient (ZPG) boundary layers. The intermittency, nondimensionalized by the

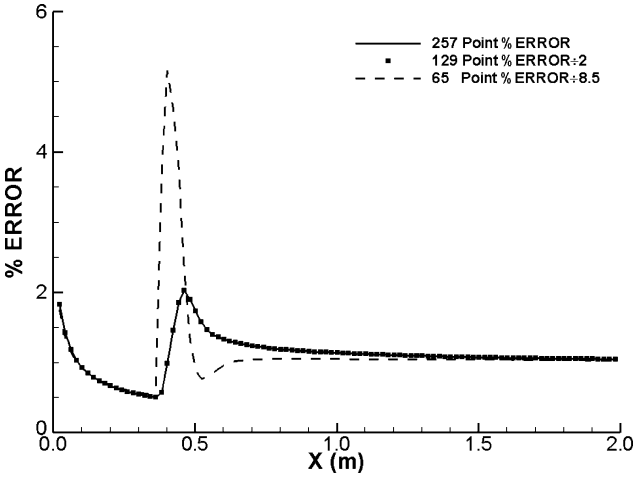

Fig. 6 Estimated grid error associated with 1×10^{-6} m near-wall spacing.

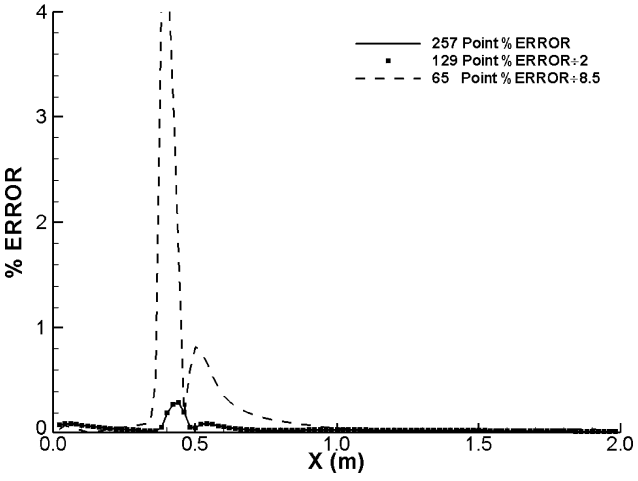

Fig. 7 Estimated grid error associated with 1×10^{-8} m near-wall spacing.

Table 2 Grid-dependency effects

Transverse points	Near-wall clustering, m	Onset location, m	Error, %	Near-wall clustering, m	Onset location, m	Error, %
257	——	0.368	0.0	——	0.368	0.0
129	10^{-6}	0.368	0.0	10^{-8}	0.368	0.0
65	——	0.356	3.2	——	0.352	4.3

definitions of Mayle,[19] is given by

$$\Gamma = \begin{cases} 1 - \exp\left[-\left(\dfrac{x - x_t}{\theta_t}\right)^2 \hat{n}\sigma\, Re_{\theta_t}^2\right] & \text{for} \quad x \geq x_t \\ 0 & \text{for} \quad x < x_t \end{cases} \tag{16}$$

where

$$\hat{n}\sigma|_{\text{ZPG}} = 1.25 \times 10^{-11} Tu^{\frac{7}{4}} \tag{17}$$

is the experimentally correlated spot production parameter for ZPG flows. One feature of this model is that the extent of transition is not required a priori. The model gradually transitions to fully turbulent flow in a manner solely dependent on the onset point variables. Also, for flows with nonzero pressure gradients (NZPG), corrections are available based on experimental data.[20] However, the simulations performed have not used any of these NZPG corrections.

Compressibility Effects on Transitional Behavior

Initial simulations of the experimental study of Mee, specifically Shot 6909/6910, are performed to examine compressibility modeling effects. From the experimental data, onset is determined to occur at approximately ≈0.4 m downstream of the leading edge. The resulting transitional prediction with use of the ZPG intermittency function of Dhawan and Narasimha is compared to the heat-transfer coefficient data of Mee in Fig. 8. Also included for comparison is a prediction assuming instant transition, that is, where Γ is set to unity instantly at the onset location whereby a fully turbulent condition is reached almost immediately. Results are reasonable but they do not reproduce the overpeaking evident in the experiment.

Suspecting compressibility modeling effects might be an issue, a simulation is performed where the compressibility correction model is eliminated. The resulting heat-transfer rate is compared to experiment in Fig. 9 and follows the expected trend but with an overestimation of heat-transfer coefficient after transition. Even so, there is better agreement during the transitional process, suggesting that some type of transition sensitive modification is required for the compressibility correction model.

The degree of compressibility with use of two-equation turbulence modeling closure techniques is typically measured through the turbulent Mach number, which is itself directly dependent on the turbulent kinetic energy (TKE). For the calculations shown in Figs. 8 and 9, the value of TKE used in calculating the turbulent Mach number, and hence, the compressibility effect, is the one assuming fully turbulent conditions, as required for reasons discussed earlier. For transitional flows, this is not appropriate. To remedy this, M_T is blended by the intermittency function, yielding a transitional turbulent Mach number defined as

$$M_T' = \Gamma M_T \tag{18}$$

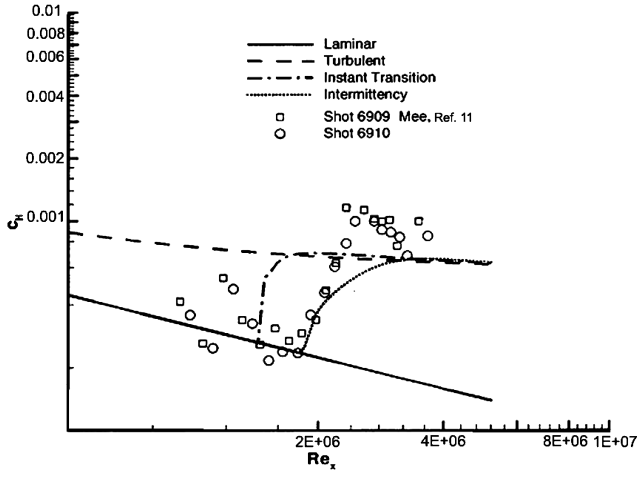

Fig. 8 Comparison of instant and intermittency blended model transition prediction to shot 6909/6910 of Mee.[11]

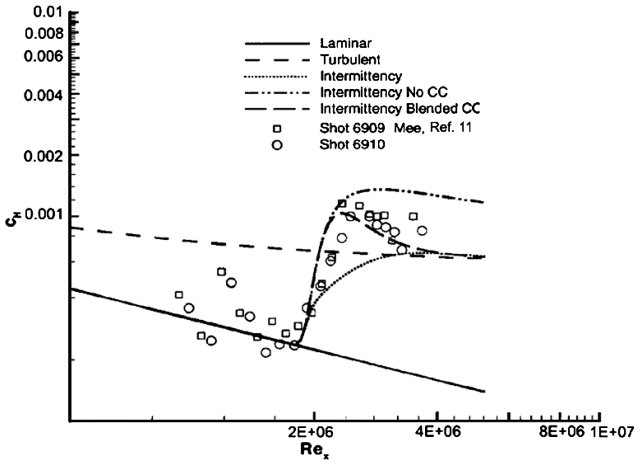

Fig. 9 Example of compressibility correction effect showing cases with full compressibility, no compressibility, and blended compressibility compared to shot 6909/6910 of Mee.[11]

Results obtained with this modification are again compared to shot 6909/6910 in Fig. 9. The overpeaking in heat transfer is now reproduced, and the value returns to the correct fully turbulent results after transition and is in much better agreement with experiment.

Transport-Based Unified Transitional Model

The algebraic methods used to determine onset and transition have several deficiencies. Most algebraic models can analyze only two-dimensional transition and are not responsive to effects of disturbances (such as those produced by shock/boundary interactions at compression corners) on the onset location. One method to address these deficiencies is to introduce a transport model that can account for more complex transition phenomena. The following sections provide a brief background of the partial differential equation (PDE) transport equation used for transition onset prediction.

The PDE transition onset transport model to be described follows directly from the work of Warren et al.[10,21] and Warren and Hassan.[22] One justification for the PDE model is to capture crossflow instabilities, which had proven difficult using stability methods. Another was that transition onset and transition to turbulence could be calculated by one continuous scheme as opposed to the several calculations and precalculations necessary for both algebraic and conventional stability methods. Yet another was to analyze transition for complex three-dimensional bodies, not readily achieved using algebraic and current stability methods.

Although the derivation of the PDE model described follows that given by Warren et al.,[10] the present version differs in several significant ways. The Warren et al. model is formulated by using either a one-equation turbulence model or the two-equation k–ζ model, whereas the present model is used within the SSGZ-J k–ε framework described earlier. Also, whereas the Warren et al. model uses a single combined TKE transport equation for both turbulence and laminar fluctuation, the present model introduces the transition onset process through a separate transport equation. Essentially, intermittency is not used to blend the two physical models into a single transport equation but rather treats the two processes (turbulence and transition) as separate modeling concerns through the use of different transport equations affording better control and calibration of the model.

The basis for obtaining a transport equation for laminar flow fluctuations leading to transition onset comes from separating the fluctuating Reynolds stress into a laminar and turbulent fluctuation component as follows:

$$(u_i'u_j') = \Gamma(u_i'u_j')_T + (1 - \Gamma)(u_i'u_j')_\ell \tag{19}$$

The fundamental assumption is that the turbulent part can be solved by using the normal k–ε transport equation, whereas the laminar component is solved by using a laminar fluctuation version of the

TKE transport equation coupled with various stability criteria. Because the laminar turbulent kinetic energy k_ℓ and turbulent kinetic energy k are parts of the same fluctuation quantity, the general form of the transport equation for k_ℓ follows that of k, namely,

$$\frac{\partial \rho k_\ell}{\partial t} + \rho u_j \frac{\partial k_\ell}{\partial x_j} - \frac{\partial}{\partial x_j}\left[\left(\mu + \frac{\mu_{T_\ell}}{\sigma_k}\right)\frac{\partial \rho k_\ell}{\partial x_j}\right] = P_{k_\ell} - D_{k_\ell} \quad (20)$$

where σ_k is taken to be the same value used in the preceding general TKE equation. The production term follows the same form as its turbulent counterpart,

$$P_{k_\ell} = \tau_{ij_\ell}\frac{\partial u_i}{\partial x_j} \quad (21)$$

except that

$$\tau_{ij_\ell} = 2\mu_{T_\ell} S_{ij} - \tfrac{2}{3}\rho k_\ell \quad (22)$$

which uses the laminar part of the turbulent eddy viscosity. The dissipation term comes from Warren and Hassan[21] and is defined as

$$D_{k_\ell} = a\left(\mu_{T_\ell}/\mu\right)\eta k_\ell \quad (23)$$

where

$$\eta = \sqrt{S_{ij}S_{ij}} \quad (24)$$

is the magnitude of the rate of strain. Transition onset is determined to be the point where $R_T = 1/C_\mu(\mu_{T_\ell}/\mu)$ exceeds unity.[22] Here, the mode disturbances grouped into μ_{T_ℓ} fulfill the role of the turbulent timescale/length scale so that no additional transport or algebraic equations are required.

The eddy viscosity associated with the laminar component of the turbulent fluctuations is defined as the sum of the first and second mode turbulent timescales,[21] or

$$\mu_{T_\ell} = C_{\mu_{T_\ell}}\rho^* k_\ell\left(\tau_{\mu_{T_{\ell_1}}} + \tau_{\mu_{T_{\ell_2}}}\right) \quad (25)$$

The first mode quantifies instabilities associated with natural transition and is based on Obremski et al.[23] and correlated by Walker.[24] The precise formula used in the present study modified for high-speed flows is defined as

$$\tau_{\mu_{\ell_1}} = (a/\omega_1)\cos\psi \quad (26)$$

where

$$\omega_1 = \left(U_e^2/v\right)3.2(Re_{\delta^*})^{\frac{-3}{2}} \quad (27)$$

$$\psi = 5.633\times 10^{-5}M_e^5 - 2.298\times 10^{-3}M_e^4 + 3.618\times 10^{-2}M_e^3 - 2.746\times 10^{-1}M_e^2 + 9.273\times 10^{-1}M_e \quad (28)$$

The symbol ψ represents the obliqueness angle reduction and is a curve fit to the freestream Mach number using the data of Mack.[25]

For supersonic flows, the second instability modes become dominant. The timescale of the second instability mode is defined as

$$\tau_{\mu_{\ell_2}} = a/\omega_2 \quad (29)$$

The frequency of the disturbance is defined as

$$\omega_2 = U_e/\lambda \quad (30)$$

From correlations by Mack[25] as well as Stetson and Kimmel,[26] the length scale of the model is on the order of two times the local boundary-layer thickness, or

$$\lambda \sim 3.5\delta \quad (31)$$

where

$$\delta \sim c\left(M_e^2 x/\sqrt{Re_x}\right) \quad (32)$$

and c is assumed be unity. Additional disturbances associated with other transition phenomena, such as transition bypass and surface roughness, can also be represented in a similar fashion.[27,28] In our work, it is assumed that freestream turbulent intensities will be low enough to neglect transition bypass.

To account for laminar compressibility effects, a reference temperature correlation from Eckert[29] is used wherever a temperature or temperature-dependent quantity is required. Consequently,

$$T^* = T_e\left(10.032M_e^2 + 0.58[T_w/T_e - 1]\right) \quad (33)$$

$$\mu^* = \mu(T^*) \quad (34)$$

$$\rho^* = \rho_e T_e/T^* \quad (35)$$

$$Re = \rho^* U_e/\mu^* \quad (36)$$

The value of the constant a was determined by Warren and Hassan,[21] through calibration with the low-speed transitional flow studies of Schubauer and Klebanoff[30] and Schubauer and Skramstad[31] and is given as

$$a = 0.069(Tu - 0.138)^2 + 0.00819 \quad (37)$$

The calibration also performed well for other experimental cases such as those of Savill.[32,33] This value is used unchanged for all present calculations in order to assess the universality of the calibration.

A summary of the framework employed for transitional modeling using the PDE onset equation with algebraic intermittency is given here:

1) For the laminar solution, solve for k_ℓ by using transport equation and find location x_t, where R_T value exceeds unity.

2) For the transitional solution, solve k–ε at all locations, suppress $\tilde{\mu}_T$ for all $x < x_t$, and apply the algebraic intermittency function Γ to μ_T for $x > x_t$.

3) Intermittency goes to unity naturally without predefined end location.

Case Studies

The hypersonic scramjet forebody experiments of Holden and Rodriguez[12] and Holden[13] as well as recent high-speed flat-plate studies of Mee[11] are used as the primary means of comparison. Both data sets come from shock-tunnel experiments where neither free stream noise nor velocity fluctuation levels were measured. A summary of the case conditions and geometry is given in Table 1. An additional validation is performed for the reentry F vehicle and represents a case where actual flight conditions exist to examine turbulence transition.

Because freestream fluctuation intensity information is unavailable for these experiments, the data itself, in conjunction with the correlations, are used to "surmise" approximate levels of initial turbulence intensities. The level required to match onset of the experiment is then evaluated to determine if it is realistic for the given tunnel and run conditions. To represent realistic flight conditions, the initial turbulence intensity is set to zero for the reentry F vehicle simulation.

Mee Shot 6909/6910

The hypersonic transition experiment of Mee is simulated with use of the new PDE transition onset transport model with the Warren and Hassan[21] calibrated constants. The sensitivity to freestream turbulence levels is significant, as it should be. The first guess was that of 0.6% corresponding to pressure fluctuation levels of around 5%. Results of this calculation are shown in Fig. 10. The predicted onset point is 0.18 m downstream of the plate leading edge and well upstream of the experiment. Lowering the turbulence intensity to a level of 0.325% produces results in better agreement with the transition onset point now at 0.67 m. This lower intensity level corresponds to a pressure fluctuation (noise) level of around 2.75%, which is within the range given by He and Morgan[34] for the T4 shock tunnel.

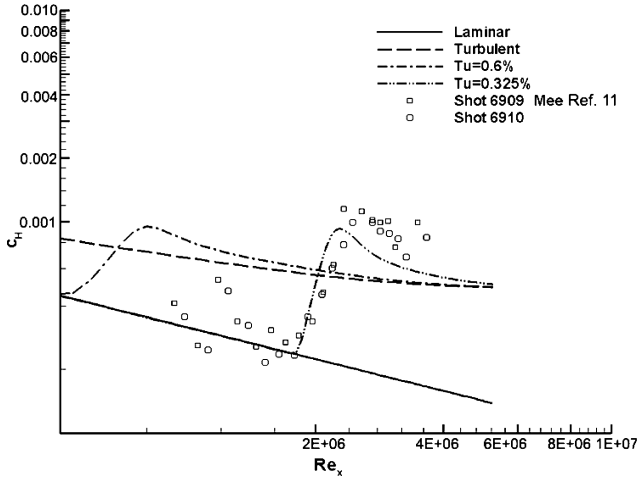

Fig. 10 Predicted heat-transfer rate with use of new onset transport model for shot 6909/6910 of Mee.[11]

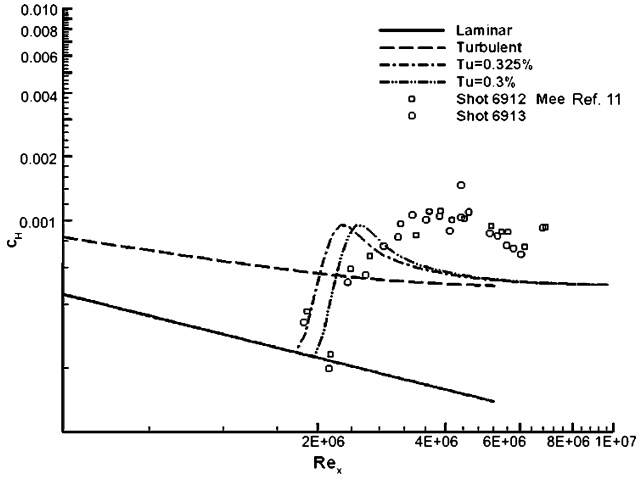

Fig. 11 Predicted heat-transfer rate with use of new onset transport model for shot 6912/6913 of Mee.[11]

Mee Shot 6912/6913

Results for shot 6912/6913 with use of the same turbulence intensity of 0.325% are shown in Fig. 11. Although the predicted onset point of 0.37 m lies between the available data points, the comparisons are not as good as for shot 6910/6911. An indication to the sensitivity of the transition onset transport model to freestream turbulence intensities is also shown in Fig. 11, where a lower freestream intensity of 0.3% moves the transition point downstream to 0.67 m.

The poor heat-transfer comparisons for the transition to turbulence and turbulent regions can largely be attributed to the algebraic transition model. A more accurate transition to turbulence model would extend the transition process. This would lengthen the transition zone and shift the peak heat-transfer rate further downstream more in line with experiment. As the focus of the present paper is largely on transition onset prediction, the algebraic model is not modified to produce more acceptable results.

Holden Compression Ramp RUN 3/5

For these simulations, a freestream intensity of 0.42% matched the data quite well with the resulting predicted heat-transfer values for runs 3/5 shown in Fig. 12. This turbulence intensity corresponds to an estimated noise level of 5.7%, in line with levels measured in similar experimental facilities.[14] Differences between the two cases are slight with an onset predicted at 1.31 m for run 3 and 1.32 m for run 5. The algebraic transition to turbulence model also does a good job of capturing the correct trend with the predicted heat-transfer data aft of transition agreeing very well with experiment.

Table 3 Reentry F vehicle flight conditions

Freestream variable	Simulation condition
Altitude	24.4 km (80,000 ft)
Mach number	19.97
Angle of attack	0.0 deg
Velocity	5948.0 m/s
Temperature	219.8 K
Density	4.583×10^{-2} kg/m^3
Pressure	2904.48 Pa
Laminar turbulent kinetic energy	1.0×10^{-10} m^2/s^2
Turbulent kinetic energy	1.0×10^{-10} m^2/s^2
Turbulent dissipation rate	1.0×10^{-9} m^2/s^3

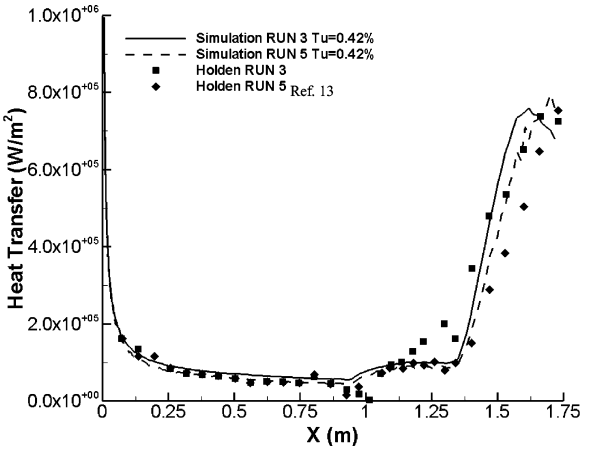

Fig. 12 Comparison of predicted heat-transfer rate with use of new onset transport model for run 3/5 of Holden.[13]

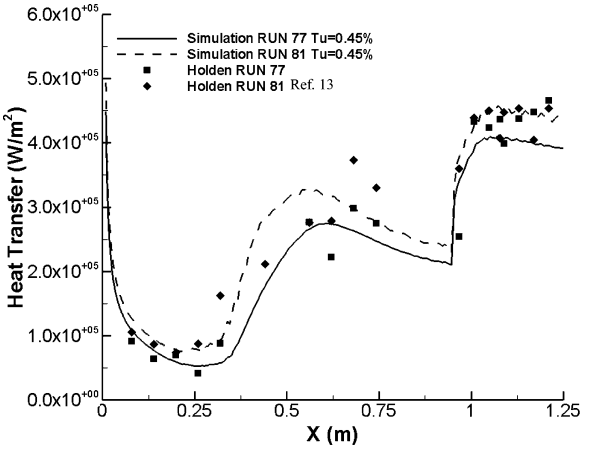

Fig. 13 Comparison of predicted heat-transfer rate with use of new onset transport model for run 77/81 of Holden.[13]

Holden Compression Ramp Run 77/81

Results for the final test case are shown in Fig. 13. Transition is predicted at 0.36 m for run 77 and 0.33 m for run 81. The correct trend as a result of turbulent transition is predicted quite well with the overall results falling within the experimental scatter. The fact that these results are obtained by using nearly the same turbulence intensity conditions (0.45%) as run 3/5 is encouraging and shows a consistency in the transition onset model.

Reentry F Vehicle

As a validation of transition for flight case conditions, a simulation of the reentry F vehicle is undertaken. Flow conditions assumed for the simulation are given in Table 3 and follow those reported by Wright and Zoby[35] for the vehicle at an altitude of 24.4 km (80,000 ft). Because the conditions are those of flight where the noise

Table 4 Case summary

Experiment	Designation	Experimental onset, m	Transport model: Turbulent intensity (noise level), %	Transport model: Onset prediction, m
Mee	Shot 6909/6910	∼0.5	0.3 (2.7)	0.7
Mee	Shot 6912/6913	∼0.4	0.3–0.33 (2.7–3.0)	0.4–0.7
Holden	Run 3	∼1.02–1.14	0.42 (5.7)	1.31
Holden	Run 5	∼1.14–1.40	0.42 (5.7)	1.31
Holden	Run 77/81	∼0.30–0.36	0.45 (4.5)	1.31–1.32
Flight case	Reentry F	∼1.5–2.0	0.0 (0.0)	1.54

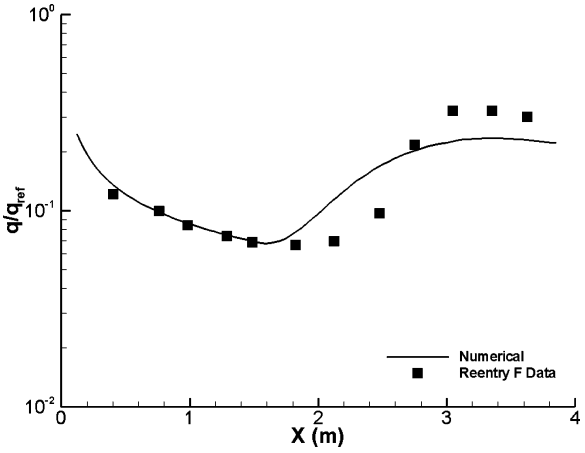

Fig. 14 Comparison of heat transfer for reentry F vehicle at 24.4 km (Ref. 37).

levels are estimated to be orders of magnitude less than experimental facilities, the initial freestream turbulence intensity employed to initialize k_ℓ is zero. The turbulence intensity utilized in the Dhawan and Narasimha transition-to-turbulence model, estimated from k_ℓ conditions at onset, is determined to be 0.001%.

The geometry is a spherical cone with a 5-deg half-angle. The nose radius of the vehicle before ablation was 2.8×10^{-3} m, whereas after ablation at the flight conditions where transition measurements were taken was estimated to be 3.43×10^{-3} m (Ref. 36). In either case, the bluntness is extremely small compared to the overall size of the vehicle (3.96 m or 13 ft). Consequently, the present simulation assumes a sharp cone. Confusion also exists as to the exact origin of the streamwise coordinate system used to define the location of transition. However, the differences are estimated to be less than 0.03 m, which is less than 3% of the measured transition location at over 1 m. As a result, the streamwise origin of the present simulation is at the tip of the vehicle. In addition, the flight case was at a slight 0.14-deg angle of attack. To stay within an axisymmetric framework, the present simulation assumes a zero angle of attack.

Comparison of heat-transfer measurements from the flight case[36] is shown in Fig. 14 (Ref. 37). There is very good agreement with the data before transition onset. Transition is predicted to occur at 1.54 m downstream of the body tip. Judging from the experimental data, this seems to be too far upstream. However, it seems that the transition process can begin near 1.5 m, as the data point at 1.8 m does not seem to follow the laminar trend. Hence, the discrepancy might be in the transition-to-turbulence model, Eq. (16), rather than the transition-onset model. Differences in heat transfer during the transition process, 1.5 to 4 m, can also be attributed to the transition-to-turbulence model, that is, not allowing the model to peak as expected.

Conclusions

Results of the simulations performed in the present study are summarized in Table 4. The comparisons that use the partial-differential-equation transition-onset model with algebraic transition-to-turbulence blending are quite reasonable. The only free parameter required in performing these simulations is an estimation of the freestream velocity fluctuation levels. The levels required to obtain acceptable results using the onset transport model are in nominal accord with the general consensus concerning noise levels in shock-tunnel facilities.[14] A significant discovery is that the results obtained by using the onset transport model required no additional calibration than that originally performed by Warran and Hassan.[21] Also, the observation that good results for several data sets are obtained with tunnel dependent noise levels [$2\frac{1}{2}$–3% for the Mee T4 study and $5\frac{1}{2}$–6% for the Holden Large Energy National Shock Tunnel (LENS) study] indicates great promise for this approach when simulating flows within these facilities. The methodology also performs quite well in predicting the transition-onset location for the flight case reentry F vehicle when using zero turbulence intensity levels consistent with flight conditions.

If anything, the overall methodology diverges from experiment largely in the area of transition to turbulence where the Dhawan and Narasimha algebraic correlation is utilized. Future work is focusing on the use of the current transport-onset model with an intermittency transport model to not only improve transition-to-turbulence prediction but also permit the simulation of more complex transitional problems such as bodies at angle of attack.

References

[1]Chang, Chau-Lyan, "The Langley Stability and Transition Analysis Code (LASTRAC): LST, Linear & Nonlinear PSE for 2-D Axisymmetric, and Infinite Swept Wing Boundary Layers," AIAA Paper 2003-0974, Jan. 2003.

[2]So, R. M. C., Sarkar, S., Gerodimos, G., and Zhang, J., "A Dissipation Rate Equation for Low-Reynolds-Number and Near-Wall Turbulence," *Theoretical Computational Fluid Dynamics*, Vol. 9, Jan. 1997, pp. 47–63.

[3]Chien, K.-Y., "Predictions of Channel and Boundary-Layer Flows with a Low-Reynolds-Number Turbulence Model," *AIAA Journal*, Vol. 20, No. 1, 1982, pp. 33–38.

[4]So, R. M. C., Zhang, H. S., and Speziale, C. G., "Near-Wall Modeling of the Dissipation Rate Equation," *AIAA Journal*, Vol. 29, No. 12, 1991, pp. 2069–2076.

[5]Papp, J. L., and Dash, S. M., "Turbulence Model Unification and Assessment for High-Speed Aeropropulsive Flows," AIAA Paper 2001-0880, Jan. 2001.

[6]Sarkar, S., "The Pressure-Dilatation Correlation in Compressible Flows," *Physics of Fluids A*, Vol. 4, No. 12, 1992, pp. 2674–2682.

[7]Zeman, O., "Dilatation Dissipation: The Concept and Application in Modeling Compressible Mixing Layers," *Physics of Fluids A*, Vol. 2, No. 2, 1990, pp. 178–188.

[8]Zeman, O., "On the Decay of Compressible Isotropic Turbulence," *Physics of Fluids A*, Vol. 3, No. 5, 1991, pp. 951–955.

[9]Berkowitz, A. M., Kyriss, C. L., and Martellucci, A., "Boundary Layer Transition Flight Test Observations," AIAA Paper 77-125, Jan. 1977.

[10]Warren, E. S., Harris, J. E., and Hassan, H. A., "Transition Model for High-Speed Flow," *AIAA Journal*, Vol. 33, No. 8, 1995, pp. 1391–1397.

[11]Mee, D. J., "Boundary Layer Transition Measurements in Hypervelocity Flows in a Shock Tunnel," AIAA Paper 2001-0208, Jan. 2001.

[12]Holden, M. C., and Rodriguez, K., "Experimental Studies of Shock Wave/Wall-Jet Interaction in Hypersonic Flows," Calspan-UB Research Center, Rept. 2610-1, Buffalo, NY, 1994.

[13]Holden, M. C., "Studies of Scramjet Performance in the LENS Facilities," AIAA Paper 2000-3604, July 2000.

[14]Schneider, S. P., "Effects of High-Speed Tunnel Noise on Laminar-Turbulent Transition," *Journal of Spacecraft and Rockets*, Vol. 38, No. 3, 2001, pp. 323–333.

[15]Goyne, C. P., "Skin Friction Measurements in High Enthalpy Flows at High Mach Number," Ph.D. Dissertation, Dept. of Mechanical Engineering, Univ. of Queensland, Brisbane, Australia, 1999.

[16]York, B. J., Kenzakowski, D. C., Lee, R. A., and Dash, S. M., "Upgrades to CRAFT Code for Simulation of Ducted Launcher/Plume Interactions," 1997 JANNAF EPTS & SPIRITS Users Group Joint Meeting, Lockheed Martin, Sunnyvale, CA, April 1997.

[17]Thompson, J. F., Warsi, Z. U. A, and Mastin, C. W., *Numerical Grid Generation: Foundation and Applications*, North-Holland, New York, 1985.

[18]Dhawan, S., and Narasimha, R., "Some Properties of Boundary Layer During the Transition from Laminar to Turbulent Flow Motion," *Journal of Fluid Mechanics*, Vol. 3, 1958, pp. 418–436.

[19]Mayle, R., "The Role of Laminar Turbulent Transition in Gas Turbine Engines," *Journal of Turbomachinery*, Vol. 113, 1991, pp. 509–537.

[20]Steelant, J., and Dick, E., "Modelling of Bypass Transition with Conditioned Navier–Stokes Equations Coupled to an Intermittency Transport Equation," *International Journal for Numerical Methods in Fluids*, Vol. 23, 1996, pp. 193–220.

[21]Warren, E. S., and Hassan, H. A., "Transition Closure Model for Predicting Transition Onset," *Journal of Aircraft*, Vol. 35, No. 5, 1998, pp. 769–775.

[22]Warren, E. S., and Hassan, H. A., "An Alternative to the e^n Method for Determining Set of Transition," AIAA Paper 97-0825, Jan. 1997.

[23]Obremski, H. J., Morkovin, M. V., and Landahl, M., "Portfolio of Stability Characteristics of Incompressible Boundary Layer," AGARDograph 134, March 1969.

[24]Walker, G. J., "Transitional Flow on Axial Turbomachine Blading," *AIAA Journal*, Vol. 27, No. 5, 1989, pp. 595–602.

[25]Mack, L. M., "Linear Stability Theory and the Problem of Supersonic Boundary-Layer Transition," *AIAA Journal*, Vol. 13, No. 3, 1975, pp. 278–289.

[26]Stetson, K. F., and Kimmel, R. L., "On Hypersonic Boundary Layer Stability," AIAA Paper 92-0737, Jan. 1992.

[27]McDaniel, R. D., and Hassan, H. A., "Role of Bypass Transition in Conventional Hypersonic Facilities," AIAA Paper 2001-0209, Jan. 2001.

[28]McDaniel, R. D., and Hassan, H. A., "Study of Bypass Transition Using the k–z Framework," AIAA Paper 2001-2310, June 2000.

[29]Eckert, E. R. G., "Engineering Relations for Heat Transfer and Friction in High-Velocity Laminar and Turbulent Boundary Layer Flow over Surfaces with Constant Pressure and Temperature," *Transactions of the American Society of Mechanical Engineers*, Vol. 78, No. 6, 1956, p. 1273.

[30]Schubauer, G. B., and Klebanoff, P. S., "Contributions on the Mechanics of Boundary-Layer Transition," NACA Rept. 1289, March 1956.

[31]Schubauer, G. B., and Skramstad, H. K., "Laminar Boundary Layer Oscillations and Transition on a Flat Plate," NACA Rept. 909, 1948.

[32]Savill, A. M., "Some Recent Progress in The Turbulence Modeling of Bypass Transition," *Near-Wall Turbulent Flows*, edited by R. M. C. So, C. G. Speziale, and B. E. Launder, Elsevier, Amsterdam, 1993, pp. 829–848.

[33]Savill, A. M., "Further Progress in The Turbulence Modeling of Bypass Transition," *Engineering Turbulence Modeling and Experiments 2*, edited by W. Rodi and F. Martelli, Elsevier, Amsterdam, 1993, pp. 583–592.

[34]He, Y., and Morgan, R. G., "Transition of Compressible High Enthalpy Boundary Layer Flow over a Flat Plate," *Aeronautical Journal*, Vol. 98, No. 972, 1994, pp. 25–34.

[35]Wright, R. L., and Zoby, E. V., "Flight Boundary-Layer Transition Measurements on Slender Cone at Mach 20, " AIAA Paper 77-719, June 1977.

[36]Wurster, K. E., Zoby, E. V., and Thompson, R. A., "Flowfield and Vehicle Parameter Influenc on Results of Engineering Aerothermal Methods," *Journal of Spacecraft and Rockets*, Vol. 28, No. 1, 1991, pp. 16–22.

[37]Howard, F. G., "Thermal Analysis Methods and Bassic Heat Transfer Data for a Turbulent Heating Flight Experiment at Mach 20 (Reentry F)," NASA TMX-2282, March 1971.

B. Hassan
Associate Editor